Computation of precise geoid model of Auvergne using current UNB Stokes-Helmert's approach

Juraj JANÁK[1], Petr VANÍČEK[2], Ismael FOROUGHI[2], Robert KINGDON[2], Michael B. SHENG[2], Marcelo C. SANTOS[2]

[1] Department of Theoretical Geodesy, Slovak University of Technology, Radlinského 11, 81005 Bratislava, Slovakia

[2] Department of Geodesy and Geomatics, University of New Brunswick, Fredericton, NB, Canada E3B 5A3; e-mail: i.foroughi@unb.ca

Abstract: The aim of this paper is to show a present state-of-the-art precise gravimetric geoid determination using the UNB Stokes-Helmert's technique in a simple schematic way. A detailed description of a practical application of this technique in the Auvergne test area is also provided. In this paper, we discuss the most problematic parts of the solution: correct application of topographic and atmospheric effects including the lateral topographical density variations, downward continuation of gravity anomalies from the Earth surface to the geoid, and the optimal incorporation of the global gravity field into the final geoid model. The final model is tested on 75 GNSS/levelling points supplied with normal Molodenskij heights, which for this investigation are transformed to rigorous orthometric heights. The standard deviation of the computed geoid model is 3.3 cm without applying any artificial improvement which is the same as that of the most accurate quasigeoid.

Key words: gravity field, geoid, Stokes-Helmert's method, downward continuation, topographical density variation, rigorous orthometric heights

1. Introduction

In 1849 G. G. Stokes introduced his method of geoid determination from gravity measurements, and his analytical solution for a spherical boundary has become known as Stokes's integral (*Stokes, 1849*). Stokes made the assumptions that we'd have measured gravity on the geoid and that there are no masses above the geoid. Neither assumption is satisfied in practice and we have to deal with them in one way or another. One reasonable idea to

overcome the problem stemming from the later assumption came from F. R. Helmert *(Helmert, 1884)* who suggested to condense all topographic masses into a 2D layer located on or below the geoid, to mathematically avoid the topographic mass issue. Helmert's approach applied to the geoid (known as the second Helmert's condensation technique) combined with the original Stokes's idea has become known in literature as the Stokes-Helmert (SH) method. During recent decades, the SH method has been developed and coded by the University of New Brunswick (UNB) Geodesy Group and is documented in many publications, e.g., (*Vaníček and Martinec, 1994; Ellmann and Vaníček, 2006*).

Similarly, the transformation of gravity observed on and above the Earth surface down to the geoid, known as downward continuation, has been studied by the UNB group. They have opted for using the physically rigorous approach formulated by Poisson (*MacMillan, 1930*) and the results of their studies of Poisson's method for the downward continuation of harmonic functions are documented in several publications, e.g., (*Vaníček et al., 1996; Sun and Vaníček, 1998; Kingdon and Vaníček, 2010*). As a by-product of their investigation they discovered that in order to downward continue a gravity anomaly, the anomaly must be of a "solid" type (*Vaníček et al., 2004*), which rules out the use of free-air as well as planar Bouguer gravity anomalies.

To reach a one-centimeter accuracy geoid model at a regional scale is a very challenging task, especially in a mountainous region. Ever since *Duquenne (2007)* produced a good standard database to test the methods of geoid or quasigeoid computation, several authors, see, e.g., (*Ågren et al., 2009, Yildiz et al., 2012*) have computed regional quasigeoid models in the Auvergne region. The quasigeoid models, presented in *Ågren et al. (2009)*, were tested at 75 GNSS/levelling points and the standard deviation of residuals (after one-parameter fitting) were all in the vicinity of 3.7 cm. It was reported in the same study that the Least Square Modification of Stokes method (LSMS or KTH approach (*Sjöberg, 2003*)) provides the best quasigeoid model among other methods (STD of 3.3 cm). In fact, this method produces geoid model, which is converted to a quasigeoid. Herein, we present a regional geoid model computed using the UNB SH method, providing a detailed description, graphical presentation of intermediate computations, testing of the final model (without any fitting),

comparison with other selected models and discussion of theoretical and practical problems and advantages of the SH method.

The second section is dedicated to the theory behind the SH method, mentioning the basic ideas in a schematic way with relevant references for readers who wish to learn the detailed theoretical arguments. Section 3 introduces the Auvergne region for which our geoid model has been computed and tested; it also gives some statistical information about the input data. Section 4 is focused on the compilation of spherical Bouguer gravity anomalies, also known as NT (No-Topography) anomalies, and on Helmert's gravity anomalies on the topography. In the next section, the downward continuation of Helmert's anomalies is presented together with the rest of the intermediate results of the geoid solution. Section 6 describes the assessment of our geoid model vis-à-vis the 75 GNSS/levelling points supplied by IGN. The last section is devoted to a brief discussion and conclusions.

2. Stokes-Helmert method, present state and references

The theory behind the UNB SH method has been described in many publications. Therefore, instead of repeating the mathematical formulae, which can be found in, e.g., (*Vaníček and Sjöberg, 1991; Vaníček and Martinec, 1994; Tenzer et al., 2003; Ellmann and Vaníček, 2006; Vaníček et al., 2013*), we have chosen to show the flow of the computation in elementary steps supplemented by brief descriptions.

$$\Delta g[r_t(\Omega).\Omega] \rightarrow \Delta g^H[r_t(\Omega).\Omega]\,. \tag{1}$$

In the first step, the observed free-air gravity anomalies are converted to Helmert gravity anomalies, one of the couple of anomalies known to be "solid" and thus capable of being continued downwards to the geoid (*Vaníček et al., 2004*). This conversion consists of adding the direct topographical and atmospheric effects (DTE) and (DAE), the secondary indirect topographical and atmospheric effects (SITE) and (SIAE) and, if the topographical density model is available, also the direct topographical density effect (DDE). All these effects, except DDE, are evaluated as sums of the near zone and far zone contributions and are computed at the locations of the observed points

on the surface of the Earth. Beside these standard corrections if the available topographical heights are of the orthometric kind, a small correction to normal gravity, called the geoid-quasigeoid correction, is also applied. In Eq. (1) and throughought this paper, Ω stands for geocentric direction, i.e., (φ, λ), the geocentric latitude and longitude; the subscripts t and g denote a radius-vector ending either at the topography or at the geoid; subscripts beside residual quantities show the degre and order of the reference field and the angular radius of the integration cap; and the meaning of the supescript H is that the superscripted quantity belongs to Helmert's space.

We refer to this step also as the transformation from the "Real space" to "Helmert's space". More details about this step can be found e.g., in (*Martinec and Vaníček, 1994a; Martinec, 1998; Vaníček et al., 1999; Novák, 2000*). Concerning lateral topographical density effect studies, see (*Martinec, 1993; Martinec et al., 1995; Huang et al., 2001*).

$$\Delta g^H[r_t(\Omega).\Omega] \to \Delta g^H[r_g(\Omega).\Omega] \,. \tag{2}$$

The second step consists only of the downward continuation of Helmert's gravity anomaly from the Earth's surface to the geoid. The UNB Geodesy Group had decided to use the most rigorous approach to downward continuation, i.e., that due to Poisson. This approach requires the gravity anomaly on the Earth surface to be "solid" and harmonic within the topography, which is indeed the case with Helmert's anomaly. This step is often considered to be somewhat problematic due to the numerical instability of the inverse Poisson integral. After a thorough theoretical and numerical investigation, e.g., (*Vaníček et al., 1996; Sun and Vaníček, 1998; Huang, 2002; Huang et al., 2003; Kingdon and Vaníček, 2010*), it was decided to use the Jacobi iterative algorithm for the solution of the inverse Poisson integral.

$$\Delta g^H[r_t(\Omega).\Omega] \to \delta\Delta g^H[r_g(\Omega).\Omega] \,. \tag{3}$$

This step consists of subtraction of the reference gravity field, (in terms of reference Helmert's gravity anomalies) of selected degree and order L resulting in residual Helmert's gravity anomalies on the geoid. Residual gravity anomalies refer to the reference spheroid of degree and order L. Before this operation is performed, the earth gravity model (satellite only EGM) used for the generation of reference gravity anomalies has to be "Helmertized", i.e., transformed to the Helmert space. For the reference, see, e.g., (*Vaníček*

and Sjöberg, 1991; Vaníček et al., 1995; Martinec and Vaníček, 1996). This transformation requires the knowledge of a global digital elevation model (DEM) in terms of spherical harmonic coefficients. Technically, a part of this step is also the application of ellipsoidal corrections correcting the effect of spherical approximation of the boundary condition. It consists of two terms corresponding to the terms of the boundary condition, which are called the ellipsoidal correction to the gravity disturbance, and the ellipsoidal correction for the spherical approximation (see *Vaníček et al., 1999*).

$$\delta \Delta g^H[r_g(\Omega).\Omega] \to \delta N^H_{L.\psi_0(\Omega)} \,. \tag{4}$$

In this step, we compute the residual Helmert cogeoid on a selected regular grid using Stokes's integration over the spherical cap of radius ψ_0, and integration kernel modified to degree L according to the idea by Molodenskij, see (*Molodenskij et al., 1960*). We note that the spatial Stokes convolution of $\delta \Delta g^H[\gamma_g(\Omega), \Omega]$ with the modified Stokes kernel is done using a UNB technique that is faster than Fast Fourier Transform methods (see *Huang et al., 2000*). The modification is selected so as to minimize the contribution from the far-zone, and by doing this to minimize the contribution from the EGM which is known to approximate the reality only in an asymptotic way. The result of this step can be called the near-zone (NZ) residual Helmert cogeoid. For details, see *Vaníček and Featherstone (1998)* and *Novák et al. (2001)*.

$$\delta N^H_{L.\psi_0}(\Omega) \to \delta N^H \,. \tag{5}$$

Here, the far-zone (FZ) contribution $\delta N^H_{L\psi_0}(\Omega)$ to the residual Helmert cogeoid, also called the "truncation error" by Molodenskij, is evaluated in a spectral way using the EGM in the Helmert space, to the appropriate degree higher than that of the reference field (L), for the chosen radius, ψ_0 and added to the NZ (spherical cap of radius ψ_0) contribution $\delta N^H_{L\psi_0}(\Omega)$. Due to the modification of the Stokes kernel, see the previous step, the truncation error term is relatively small. The result of this step is the total residual Helmert cogeoid. More details are found in (*Molodenskij et al., 1960; Vaníček and Featherstone, 1998*).

$$\delta N^H(\Omega) \to N^H(\Omega) \,. \tag{6}$$

The last step conducted in the Helmert space is the transformation of the total residual cogeoid to the complete Helmert cogeoid. This is done simply by adding to the residual cogeoid the "Helmertized" reference spheroid of degree L.

$$\delta N^H(\Omega) \to N(\Omega)\,. \tag{7}$$

The final step of the computation is the transformation of the Helmert cogeoid $N^H(\Omega)$ from Helmert space back to the real space. This is done by adding to the Helmert cogeoid the primary indirect topographical and atmospheric effects (PITE) and (PIAE) and, if the variations of topographical density are known, the primary indirect topographical density effect (PIDE). For details see *Martinec and Vaníček (1994b)* and *Martinec et al. (1996)*. As a part of this step, to preserve the physical correctness of the solution, a small correction due to the shift of the centre of mass of the Earth during the Helmert condensation needs to be applied. This correction is referred to as the Hörmander correction and it reaches up to a few centimetres. For details see *Hörmander (1976), Martinec (1998)*, and *Vaníček et al. (2013)*.

3. Input data sets

The overall quality of the geoid model depends directly on the quality of the input data. The geoid model is also affected by other errors coming from various approximations, inconsistencies when merging several data sources, numerical errors due to discretization, interpolation and integration or errors caused by unsatisfied assumptions. The aim of this section is to list the input data used in our geoid computation and provide the original reference and the accuracy, if available.

The main input to our geoid model is the free-air gravity anomaly data set based on the Burreau Gravimétrique International (BGI) gravity database originally supplied by the Bureau de Recherches Géologiques et Miničres and provided to us by the Institut Géographique National (IGN) (*Duquenne, 2007*).

It contains 244,009 values of the free-air gravity anomalies in the IGSN71 gravity reference system, with horizontal positions (ellipsoidal latitude and longitude) compatible with the ETRS89 terrestrial reference system and

the heights of the normal variety (*Duquenne, 2007*). It covers the area $43° \leq \varphi \leq 49°, -1° \leq \lambda \leq 7°$, see Fig. 1, and the standard deviation of these data, according to *Duquenne (2007)* ranges from 0.25 to 0.75 mGal. This error can increase to 1 to 2 mGal after computation of gravity anomalies, mainly due to inaccuracy in a horizontal position of the gravity points. Most of the gravity values were measured before 1971 and transformed to IGSN71 from older gravity systems. The density of the gravity data coverage varies significantly in the south-eastern part of the area, see Fig. 1. In some areas, even in the central part, the coverage is not sufficient for interpolation to a dense grid. The map of the free-air gravity anomalies is shown in Fig. 2, and the corresponding basic statistical values are listed in Table 1.

We decided to check this gravity database for outliers and duplicate points. 118 couples of duplicate points and 2 outliers were detected and eliminated.
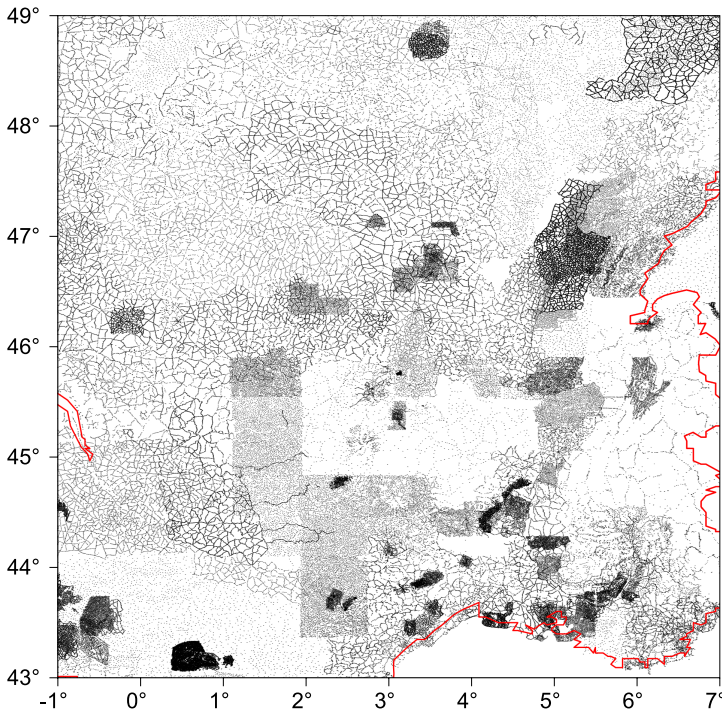
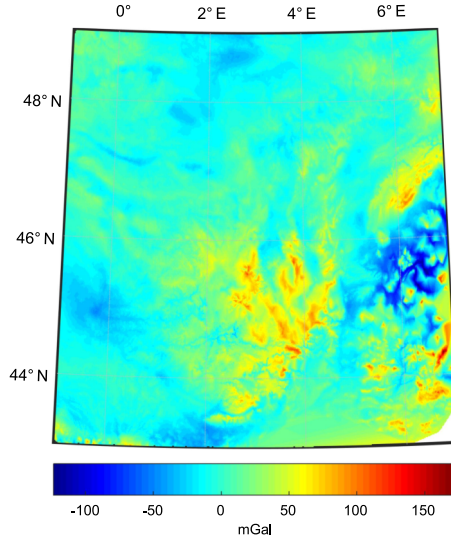

Fig. 1. Distribution of the free-air gravity anomalies.

Fig. 2. Free-air gravity anomalies directly gridded from the original scattered data based on (*Duquenne, 2007*) database.

Table 1. Statistical values of the observed (scattered) free-air gravity anomalies and normal heights at the 244009 measured points of the data set (*Duquenne, 2007*).

Quantity	Min	Max	Mean	STD
Δg (mGal)	−127.47	177.82	3.06	20.70
H_n (m)	0.00	2677.27	288.24	234.14

Another type of data set are DEMs. For our computation, we used three DEMs: the SRTM3 version 4 (*Werner, 2001; Rodriguez et al., 2005; Reuter et al., 2007*), the ACE2 which is based on a combination of the SRTM and Satellite Radar Altimetry data (*Berry et al., 2010*) and a global DEM in the form of spherical harmonic coefficients of the JGP95 model (*Lemoine et al., 1998*). The SRTM3 model was used for representing a detailed topography on a grid of $3'' \times 3''$ spacing. It was used mainly for interpolation of the free-air gravity anomalies to get free-air anomalies on a regular grid with $1' \times 1'$ resolution and for the computation of the direct topographical effect, as explained in section 4. This is a nearly global high resolution DEM with an absolute vertical error (a linear error with respect to true elevation at 90% probability) of less than 16 m (*Hensley et al., 2000; Farr et al., 2007*).

Several studies show that this error is actually smaller – about 9 meters, e.g., *Denker (2004), Rodriguez et al. (2005).* Some known problems such as the data void due to shadowing and smooth surfaces, or weak penetration of the vegetation canopies were addressed to some extent in version 4 (*Reuter et al., 2007*).

The ACE2 model is applied in those computations where the mean elevations on a grid of $30'' \times 30''$, $5' \times 5'$ or $1° \times 1°$ resolution are needed, see sections 4 and 5. For accuracy assessment of ACE2 model, see (*Berry et al., 2010*). Finally, the JGP95 model is needed in the "Helmerization" of the reference field, see section 5. A comparison with the GLOBE global DEM and accuracy assessment of this model can be found in, e.g., *Berry (1999).* The topography on a grid of $30'' \times 30''$ based on the ACE2 DEM over the area covered by terrestrial gravity data is depicted in Fig. 3.

The next input needed in our computational scheme is an Earth gravity model (EGM). The satellite-only EGM GO CONS GCF 2 DIR R5 is used for our reference field computation, see section 5. Figures of the reference gravity anomalies and the associated reference spheroid are presented in section 5.
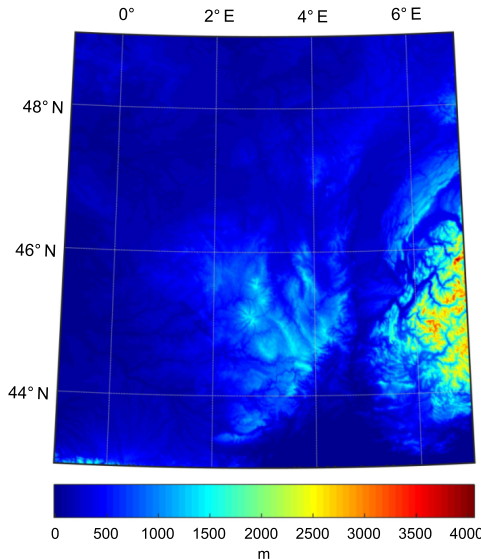

Fig. 3. Topography of the area covered by terrestrial gravity data with the resolution of $30'' \times 30''$ based on the ACE2 digital elevation model.

209

The last input used in the UNB SH-scheme is a digital topographical density model (DDM). The largest contribution comes from lateral inhomogeneity and this was the one we concentrated on here. We prepared our own lateral DDM based on an analogous geological map of France by *Bodelle et al. (1980)*, as was also investigated by *Foroughi et al. (2015b)*, that despite the low resolution of the map improves the accuracy of the gravimetric geoid in Auvergne. The DDM affects the direct topographic effect, and the primary and secondary indirect topographic effects. However, the influence on the secondary indirect topographic effect is usually negligible and was therefore not evaluated. The two remaining effects, called the direct density effect (DDE) and primary indirect density effect (PIDE) are shown in subsection 5.2. Details about the preparation and testing of the DDE for the Auvergne and surrounding area can be found in *Foroughi et al. (2015b)*.

4. Interpolation of free-air gravity anomalies on topography

The observed free-air gravity anomalies are scattered irregularly on the Earth surface. Most geoid computation algorithms, including ours, require an input of free-air gravity anomalies on a regular grid. Therefore, an interpolation of free-air gravity anomalies, which is not a trivial task, has to be performed. A procedure published by *Janák and Vaníček (2005)* was adopted. The scattered free-air gravity anomalies were transformed first into refined spherical Bouguer gravity anomalies, which are locally smooth enough to make interpolation easier. Interpolation of these anomalies into a regular geographical $1' \times 1'$ grid, see Fig. 4, was performed by the Kriging method with a linear variogram assuming an anisotropy factor due to the convergence of meridians. The basic statistical values of both scattered and interpolated refined spherical Bouguer gravity anomalies are shown in Table 2.

Free-air gravity anomalies on the same geographical grid of $1' \times 1'$ (see Fig. 5), were obtained by adding back the topographical mass effect with the elevation of the grid nodes and the shape of the surrounding terrain were taken from the SRTM3 DEM. Basic statistics are shown in the last row of Table 2.
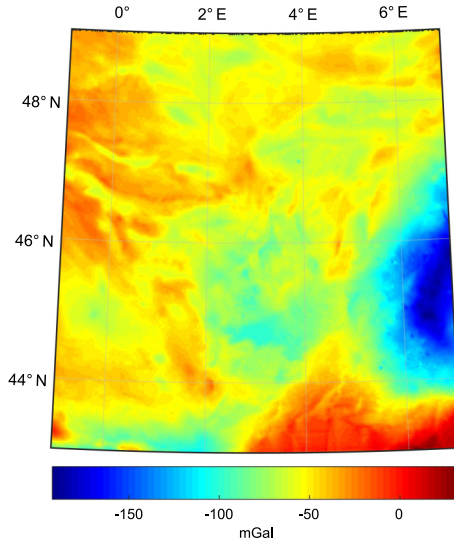
Fig. 4. Refined spherical Bouguer gravity anomalies on the Earth surface interpolated to $1' \times 1'$ geographical grid.

Table 2. Statistics of the 243889 scattered and $1' \times 1'$ interpolated refined spherical Bouguer gravity anomalies and free-air gravity anomalies.

Quantity	Min	Max	Mean	STD
Δg_{scatt} (mGal)	−127.47	177.82	3.06	20.70
$\Delta g_{RB\,scatt}$ (mGal)	−193.66	28.44	−56.74	19.95
$\Delta g_{RB\,grid}$ (mGal)	−192.87	28.50	−59.98	28.50
Δg_{grid} (mGal)	−111.36	292.33	8.82	29.03

The process of interpolation of free-air gravity anomalies can be written schematically as $\Delta g[r_t(\Omega), \Omega] \rightarrow \Delta g_{RB}[r_t(\Omega), \Omega] \rightarrow (\Delta g_{EB})_y \rightarrow (\Delta g)_y$.

5. Computation of geoid model

In this section, we present the intermediate and final results of the SH geoid computation process following the computational steps outlined in Section 2. *Foroughi et al. (2017a)* suggested a numerical technique to arrive at the optimal degree/order of reference field (this equals also the modification of Stokes's integral) and Stokes's integration radius to compute cogeoid heights. They suggested to vary the degree of reference filed and Stokes's
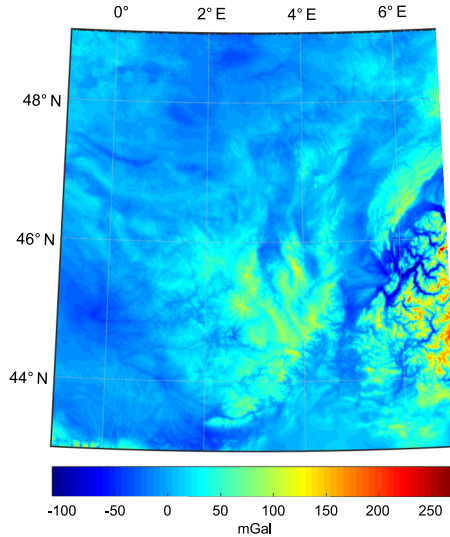
Fig. 5. Free-air gravity anomalies on a regular $1' \times 1'$ geographical grid obtained from interpolated refined spherical Bouguer gravity anomalies.

integration cap size and evaluate the final geoid with GNSS/Levelling points. In case gravity data in surrounding areas are needed when using larger integration cap sizes, they can be filled with EGM-generated grid points (*Foroughi et al., 2015a*). According to their investigation, the degree/order of 160 for the reference field and integration radius of 45' gives the best results in the sense of fitting the geoidal heights with GNSS/Levelling points in the area of Auvergne. We adopted these parameters for our study but it should be stated that these parameters can differ for different areas.

5.1 Geoid model under the assumption of standard topographic density

In order to transfer the free-air gravity anomalies to Helmert space, and thus to obtain the Helmert gravity anomalies, the effects DTE and SITE and DAE (see step 1 in Section 2) have to be applied to free-air gravity anomalies. The secondary indirect atmospheric effect, the SIAE, can safely be neglected, as its magnitude is exceedingly small. The other three effects are shown in Figs 6 and 7 and their statistical values are presented in Table 3.
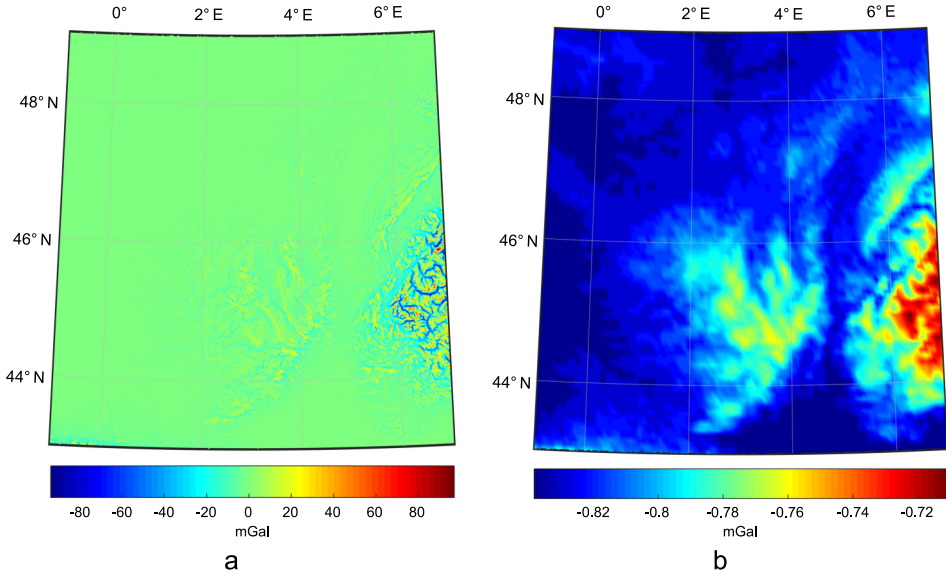
Fig. 6. Direct topographical effect (a) and direct atmospheric effect (b) used for transformation of the free-air gravity anomalies to the Helmert space.

Table 3. Statistics of Helmertization terms (mGal).

Quantity	Min	Max	Mean	STD
DTE	−103.61	110.41	−1.01	7.57
SITE	−2.23	0.00	−0.03	0.10
DAE	−0.84	−0.71	−0.82	0.02

Helmert's gravity anomalies multiplied by geocentric radius r can be continued down from the Earth surface to the geoid as they are a harmonic function. For this downward continuation, we used the Jacobi iterative procedure complemented by the determination of the maximum necessary number of iterations, as discussed by *Kingdon and Vaníček (2010)* and described in step #2 of section 2 above. Fig. 8a displays the Helmert gravity anomalies on the Earth surface and Fig. 8b shows the Helmert gravity anomalies on the geoid after applying the downward continuation.

The reference gravity anomalies in Helmert's space were computed by means of the DIR R5 up to degree/order 160 and the global digital terrain model JGP95 using the linear and quadratic coefficients, see Fig. 9a. Sub-
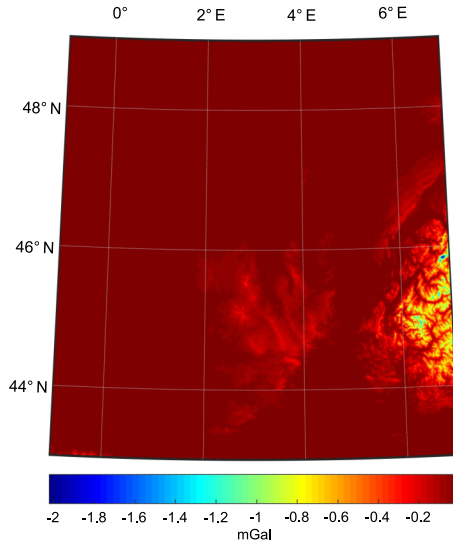
213

Fig. 7. Secondary indirect topographic effect used for the transformation of the free-air gravity anomalies to the Helmert space.
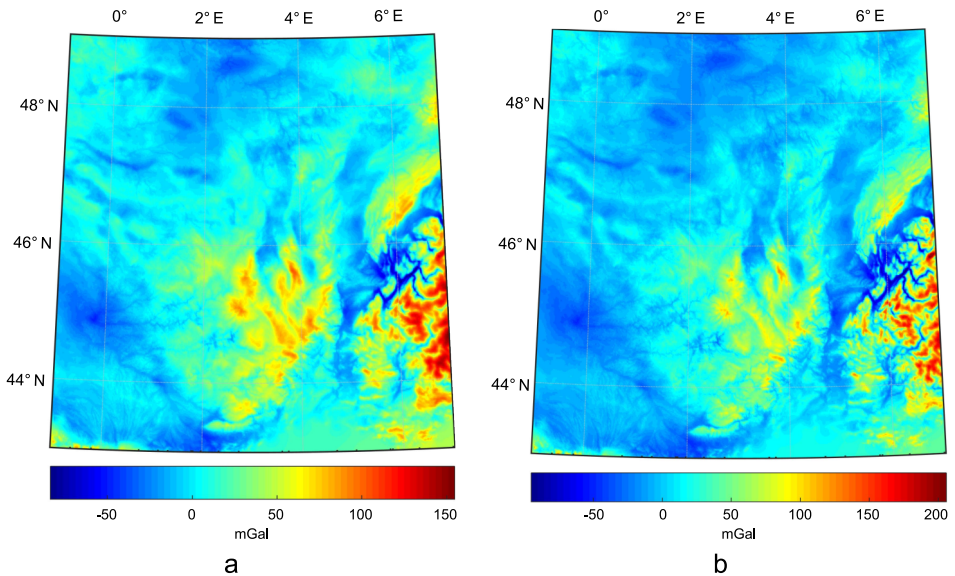

Fig. 8. Helmert's gravity anomalies on the Earth surface (a) and on the geoid (b).

Table 4. Statistics of Helmert's gravity anomalies on the earth surface and on the geoid (mGal).

Quantity	Min	Max	Mean	STD
Helmert gravity anomalies on surface	−86.82	155.08	9.84	27.36
Helmert gravity anomalies on geoid	−97.92	208.50	10.52	30.17

tracting the reference Helmert gravity anomalies from the Helmert gravity anomalies on the geoid, as obtained from terrestrial gravity measurements, we get the residual Helmert gravity anomalies, as demanded by step #3 in section 2 above, see Fig. 9b. These anomalies are further corrected by adding two ellipsoidal corrections due to spherical approximation of the boundary condition, see Figs 10a and 10b.
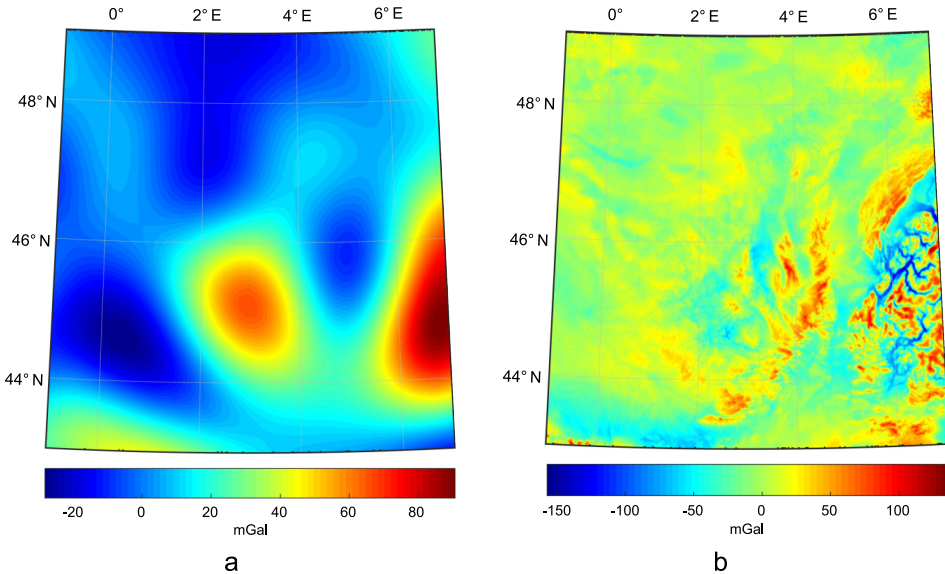

Fig. 9. Reference Helmert's gravity anomalies computed using DIR-R5 up to degree/order 160 (a) and residual Helmert's gravity anomalies (b).

Table 5. Statistics of reference Helmert's gravity anomalies and residual Helmert's gravity anomalies (mGal).

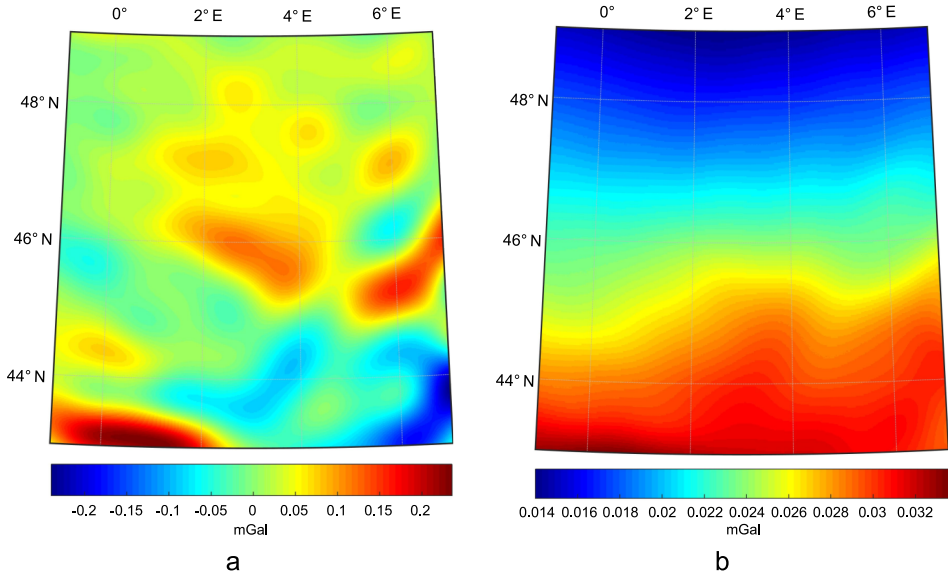| Quantity	Min	Max	Mean	STD
Reference Helmert gravity anomaly	−28.04	90.63	11.31	22.35
Residual Helmert gravity anomaly	−161.69	138.47	−0.75	23.71

Fig. 10. Ellipsoidal corrections: correction to gravity disturbance (a) and correction for spherical approximation (b).

Table 6. Statistics of ellipsoidal corrections (mGal).

Quantity	Min	Max	Mean	STD
Ellipsoidal correction to gravity disturbance	−0.239	0.235	0.019	0.059
Ellipsoidal correction to spherical approximation	0.014	0.034	0.023	0.005

Applying the Stokes integration to the residual Helmert gravity anomalies, the residual NZ co-geoid was computed at the nodal points of $1' \times 1'$ grid using modified Stokes's convolution integral (integration cap $\psi = 45'$, modification degree of 160) in $2° \times 3°$ central area, $45° < \varphi < 47°, 1.5° < \lambda < 4.5°$, in which all the GNSS/Levelling points are located. For this integration, the UNB "Faster than the FFT" technique was employed as already mentioned in step #4 in section 2 above.

The FZ contribution, a.k.a., the truncation correction (or truncation error with the opposite sign), was then evaluated from DIR-R5 using spherical harmonic coefficients (transformed into the Helmert space) of degree/order 161 up to full degree/order (300). This contribution is shown in Fig. 12a.

The low frequency part of the co-geoid, the reference spheroid, as well as the truncation correction must be added to residual co-geoid values to get the co-geoid (cf., step #6 in section 2 above), i.e., the geoid in Helmert's space, which contains all harmonic frequencies. The reference spheroid was computed using the DIR-R5 and JGP95 models up to the same degree/order 160 as for the reference Helmert gravity anomaly. Fig. 11a shows the undulation of the reference spheroid and Fig. 11b the residual co-geoid in the central area of the Auvergne region. The statistics are presented in Table 7.
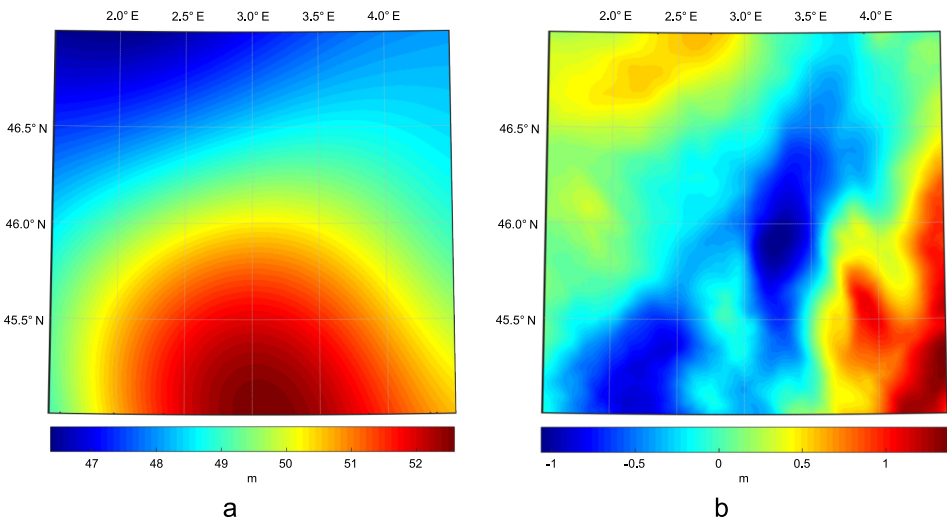

Fig. 11. Reference Spheroid computed using DIR-R5 model and up to degree/order 160 in Helmert's space (a) and residual co-geoid (b).

Transformation of the co-geoid in a Helmert space to the geoid in a real space needs to be done by applying the primary indirect topographical and atmospheric effects, the PITE and PIAE (step #7 in section 2 above), see Fig. 13. These effects were computed using the ACE2 digital terrain model. At the end of the computation process a Hörmander correction which corrects for the small shift of the centre of the Earth mass during the Helmert condensation needs to be computed (step #7 in section 2 above), see Fig. 12b and Table 7. The residual co-geoid, reference spheroid, truncation correction and all other correction terms were computed at the nodal points of $1' \times 1'$ regular geographical grid.
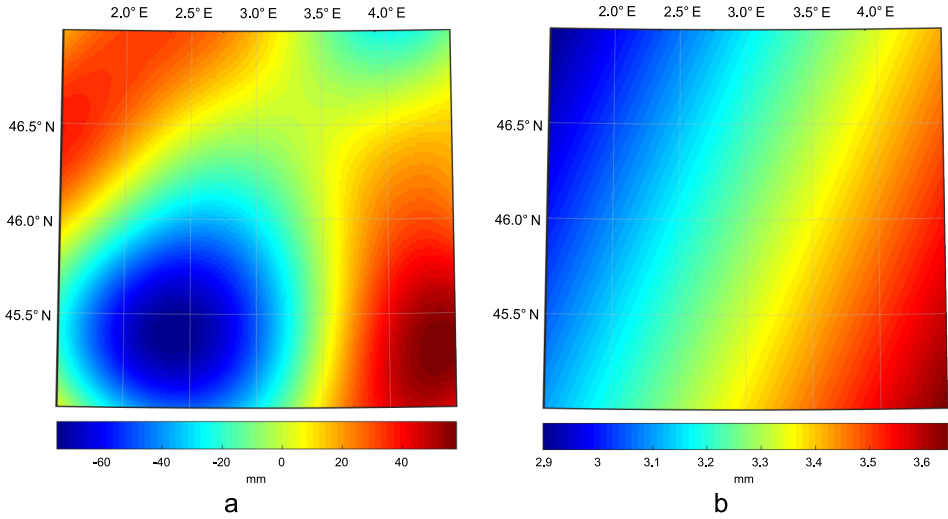
217

Fig. 12. Far-zone contribution to residual NZ co-geoid, a.k.a., truncation correction (a) and Hörmander correction (b).
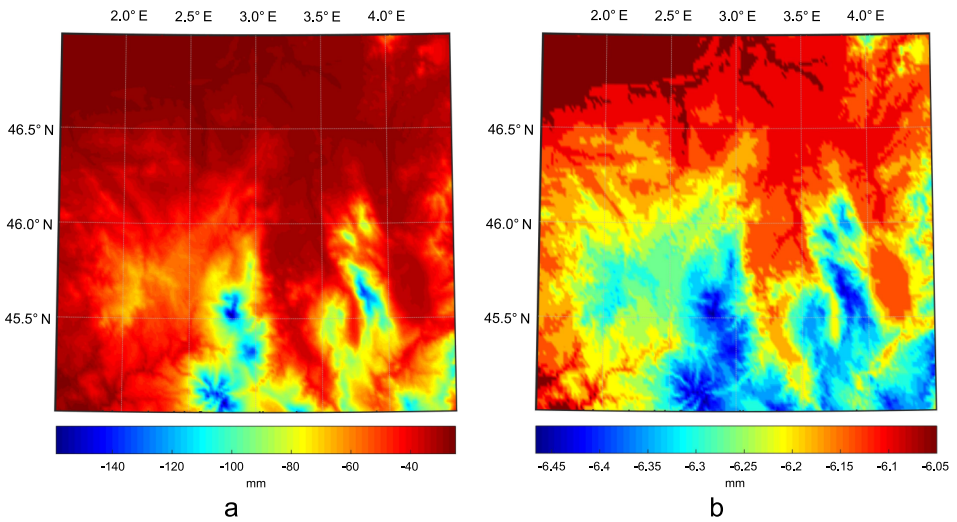

Fig. 13. Primary indirect topographical effect (a) and primary indirect atmospheric effect (b).

Final geoid model was obtained by the summation of the co-geoid, the two primary indirect effects PITE and PIAE and the Hörmander correction.

The geoid height in this area varies between 46.62m and 52.53m, see Table 7. Fig. 14 shows the geoid height variation in the computation area.

Table 7. Statistics of final geoid computation components (m).

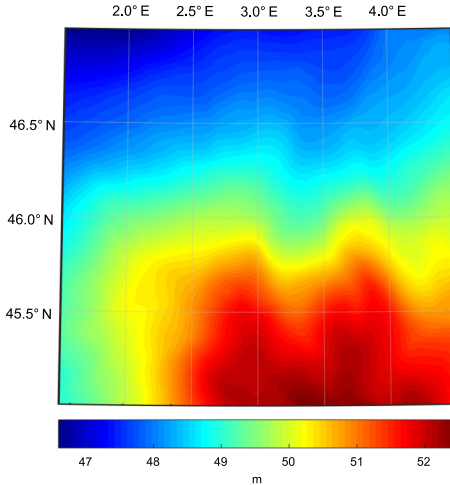| Quantity	Min	Max	Mean	STD
Reference Spheroid	46.371	52.587	49.560	1.570
Residual Co-geoid	−1.063	1.366	0.00	0.479
Truncation correction	−0.075	0.058	-0.004	0.032
PITE	−0.159	−0.025	−0.044	0.020
PIAE	−0.007	−0.006	−0.006	0.000
Hörmander correction	0.003	0.004	0.003	0.000
Geoid	46.595	52.480	49.512	1.487

Fig. 14. Geoid model in the Auvergne area assuming the standard density of topographic masses $2670\,\mathrm{kg\,m^{-3}}$.

5.2 The effect of lateral topographical density variations on the geoid

Lateral topographical density variations in this area were estimated from surface geology on a $5' \times 5'$ grid from publicly available geological map introduced in section 3. The effect of these approximate density variations on the geoid were computed in two terms of direct density effect DDE (cf.,

step #1 in section 2 above) and primary indirect density effect PIDE (cf., step #7 in section 2 above). The total effect of lateral topographical density varies between –5.8 and 2.4 cm. These corrections were applied to the final geoid model in Auvergne area; for more details see (*Foroughi et al., 2015b*). Fig. 15 shows the effects of lateral density variation on the geoid in the Auvergne area. Due to the lack of accurate density information the lateral topographical density model was created on a relatively coarse grid and thus the contribution to the geoid has been evaluated only approximately. The statistics of both components and the geoid model assuming the density variation is shown in Table 8.
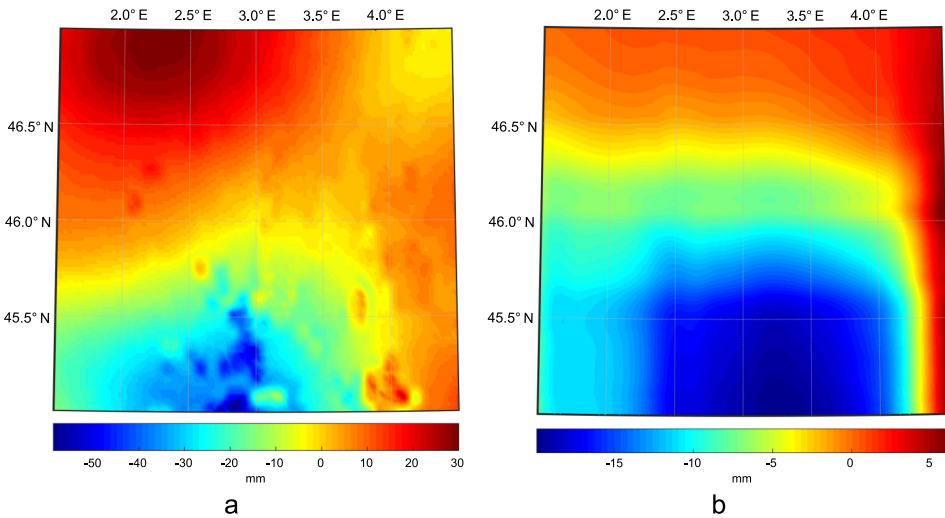

Fig. 15. Effects of lateral topographical density variations in Auvergne area: direct topographical density effect (a) and primary indirect topographical density effect (b).

Table 8. Statistics of the direct and primary indirect density effects on the geoid and statistics of the geoid model assuming the lateral topographical density variation (m).

Quantity	Min	Max	Mean	STD
DDE	−0.059	0.030	0.000	0.016
PIDE	−0.020	0.006	−0.007	0.007
Geoid	46.620	52.492	49.528	1.491

6. Testing and comparison

The 75 points on which both the GNSS-determined geodetic heights and levelled heights, expressed as "normal heights", are located in the area of Auvergne, (*Duquenne, 2007*). These points have been used for the assessment of our geoid model. First, the rigorous orthometric heights were calculated from the normal Molodensky heights based on the theory published by *Santos et al. (2006)*. The implementation of this transformation is described by *Foroughi et al. (2017b)*. The locations of these control points over the test area are shown in Fig. 16. The statistics of the differences between the two heights, rigorous orthometric minus normal, is shown in Table 9.

After obtaining the set of the rigorous orthometric heights, the geoid heights were evaluated at the location of the 75 control points, and the differ-
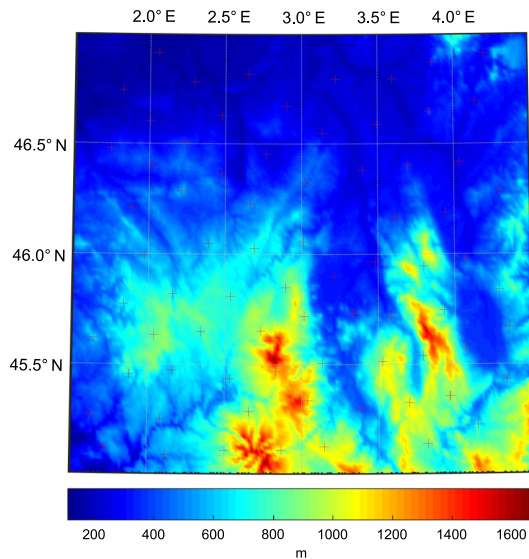

Fig. 16. Topography over the Auvergne area and locations of control GNSS/levelling points.

Table 9. Statistics of differences between the rigorous orthometric and normal heights (mm).

Quantity	Min	Max	Mean	STD	Range
$H^0 - H^n$	1.6	70.4	22.3	14.7	68.8

ences between the gravimetric geoid heights and the differences of geodetic and rigorous orthometric heights at these points were computed. These differences are characterized by the standard deviation of 3.4 cm and the mean difference of 12.4 cm, see Table 10. After the effects of lateral topographical density variation were added to the final geoid model, the comparison showed 1.4 mm improvement in the standard deviation and 7.3 mm change in the mean difference, see Table 10. Fig. 17 shows the differences between the final geoid model and the GNSS/levelling control points.

Table 10. Statistics of differences between the gravimetric geoid heights and GNSS/ levelling geoidal heights computed at 75 control points (m).

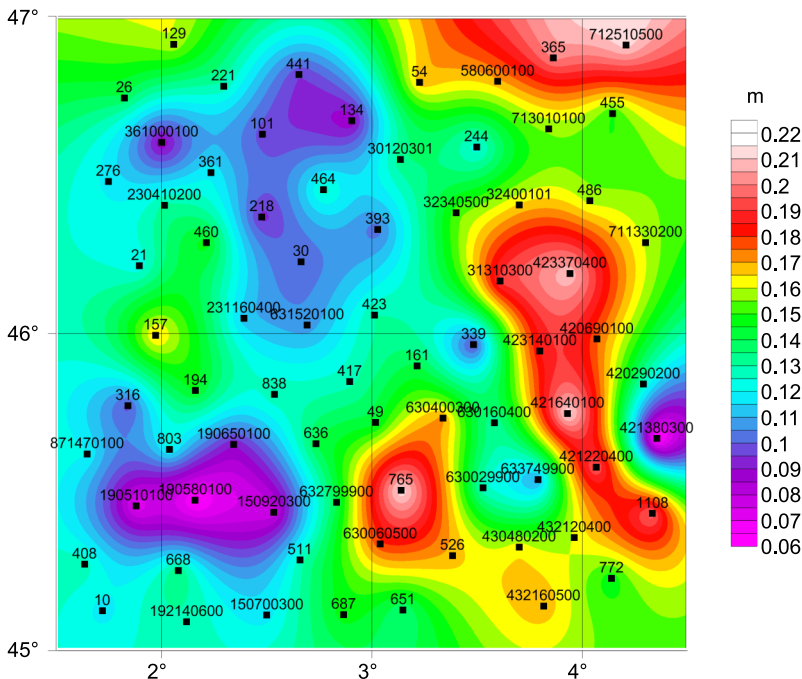| Quantity	Min	Max	Mean	STD	Range
Geoid	0.028	0.207	0.124	0.034	0.178
Geoid (density effect included)	0.024	0.222	0.133	0.033	0.197

Fig. 17. Map of differences between the gravimetric geoid model that includes the lateral topographical density effect and GNSS/levelling geoid heights at control points.

The same evaluation was done in *Ågren et al. (2009)* for their quasi-geoid solution using five different methods and normal heights of the same 75 control points – cf., *Ågren et al. (2009)*. According to their results the KTH method *Sjöberg (2003)* gives the smallest standard deviation (3.3 cm) when one-parameter corrector plane is applied. This confirms our results presented here as the KTH method is basically a simplified geoid determination (using Stokes's technique) which is then converted to quasigeoid for comparison with normal heights. However, the comparison of mean of differences is not possible since the quasigeoid results are always presented after applying a corrector surface.

More detailed statistical information about the differences can be seen from the histograms plotted in Fig. 18.
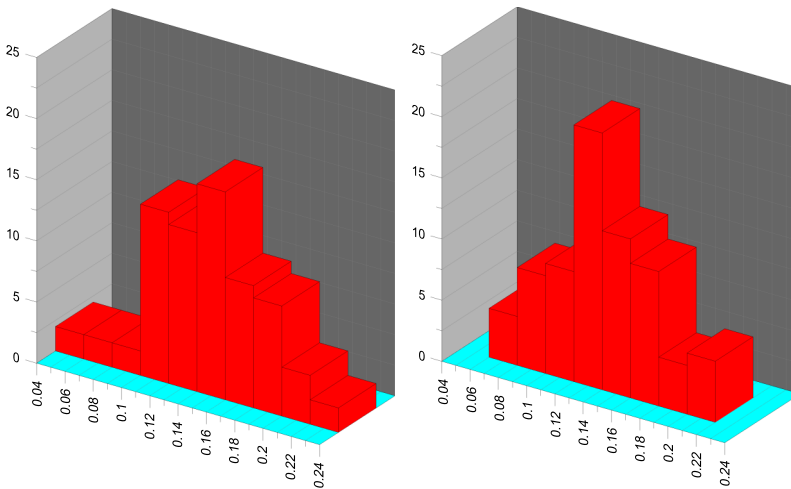

Fig. 18. Histograms of differences between the gravimetric geoid heights (standard density – left; lateral topographical density variation included – right) and GNSS/levelling geoid heights at 75 control points.

From the histograms shown in Fig. 18 it can be seen that there has been an improvement in the distribution of the differences in spite of very poor resolution of the digital density model that was used for the computation. The histogram on the right appears to be more normally distributed around the mean value.

7. Discussion and conclusions

As stated in the abstract, the intention of this paper is to show how the current version of the Stokes-Helmert geoid determination technique works with real data at least as well as the quasigeoid determination techniques do. The S-H's technique, as a result of several decades of investigation and refinements performed mainly at the University of New Brunswick was already tested on an Australian synthetic gravity field constructed at the Curtin University (*Baran et al., 2006*). The test was not very successful because the synthetic field lacked the required accuracy and self-consistency. However, it confirmed the hypothesis that the S-H theory is accurate to about 2.5 cm (standard deviation) and to a range of 20 cm when used with errorless data (*Vaníček et al., 2013*) Assuming that the errors in the SH theory (and in the code) are independent of the errors in input data, we would deduce that the effect of the data errors (observed gravity, topographical heights, topographical density, levelled heights and GNSS determined geodetic heights) combined is about 2.6 cm which is less than one should expect.

Our study in the Auvergne test region revealed, without employing any beautification technique such as corrector surfaces, and with a very inaccurate evaluation of the topographical density contribution, that the gravimetric geoid can certainly be determined to the same accuracy as, if not a better accuracy than, quasigeoid models in the same area, (see, e.g., *Yildiz et al., 2012*). This also demonstrates the successful application of Helmert's second condensation technique (see, e.g., *Martinec, 1998*), which generates very small indirect topographical effects. Moreover, it substantially reduces the requirement of knowing the topographic mass-density distribution, as the error in density committed in the topographical effect is to a large extent compensated by the error produced in the condensed topographical effect. Therefore, reasonable results can be obtained even when a standard density assumption or a coarse density model is used. However, we believe, that the presented geoid model can be further improved with finer digital density model, if it becomes available.

The mean value of our geoid solution is 13.3 cm above the average of GNSS/levelling values. This corresponds very well with the estimated constant height system offset for France which is −13.2 cm according to

Rülke et al. (2012, Table 3). This result is also an important topic for further discussion as we believe that the mean value of computed gravimetric geoid model compared to the GNSS/levelling geoidal heights can be a useful information on the used height system.

Last but not least, we would like to emphasize the importance of the physical rigor in the choice of the computation techniques. This is especially true of the most problematic step of the geoid computation procedure, the downward continuation. This task is in the background of the motivation for using the Helmert space, where we construct gravity functionals which are harmonic above the geoid (to the extent to which the assumed topographical density is known) and can therefore be continued downward rigorously using the Poisson technique. The numerical evaluation of this step is widely discussed, mainly due to its numerical instability, but the results obtained in our experiment show that it is possible to evaluate this step with a reasonable accuracy even for data on $1' \times 1'$ mesh.

References

Ågren J., Barzagi R., Carrion D., Denker H., Grigoriados V. N., KIamehr R., Sona G., Tscherning C. C., Tziavos I. N., 2009: Different geoid computation methods applied on a test data set: results and considerations. Poster presented at Hotine-Marrussi Symp., Rome, 6–12 July, 2009.

Baran I., Kuhn M., Claessens S. J., Featherstone W. F., Holmes S. A., Vaníček P., 2006: A synthetic Earth gravity model designed specifically for testing regional gravimetric geoid determination algorithms. J. Geodesy, **80**, 1–16, `doi: 10.1007/s00190-005-0002-z`.

Berry PAM, 1999: Global digital elevation models – fact or fiction? Astron. Geophys., **40**, 3.10–3.13, `doi: 10.1093/astrog/40.3.3.10`.

Berry P. A. M., Smith R. G., Benveniste J., 2010: ACE2: The new global digital elevation model. In: Gravity, Geoid and Earth Observation. IAG Symposia 135, Mertikas S. P. (ed), Springer, Berlin: 231–237. `doi: 10.1007/978-3-642-10634-7-30`.

Bodelle et al., 1980: Carte géologique de la France et de la marge continentale, 1:1500 000, 1978–1979.

Denker S., 2004: Evaluation of SRTM3 and GTOPO30 terrain data in Germany. In: Gravity, Geoid and Space Misisions. IAG Symposia 129, Jekeli C. et al. (eds), Springer, Berlin, 218–223.

Duquenne H., 2007: A data set to test geoid computation methods. Proceedings of the 1st Internatiaonal Symposium of the International Gravity Field Service (IGFS), Istambul, Turkey. Harita Dergisi, Special Issue **18**, 61–65.

Ellmann A., Vaníček P., 2006: UNB application of Stokes-Helmert's approach to geoid computation. J. Geodyn., **43**, 200–213.

Farr T. G., Rosen P. A., Caro E., Crippen R., Duren R., Hensley S.,Kobrick M., Paller M., Rodriguez E., Roth L., Seal D., Shaffer S., Shimada J., Umland J., Werner M., Oskin M., Burbank D., Alsdorf D., 2007: The Shuttle Radar Topography Mission. Rev. Geophys., **45**, RG2004, `doi: 10.1029/2005RG000183`.

Foroughi I., Janák J., Kingdon R. W., Sheng M. B., Santos M. C., Vaníček P., 2015a: Illustration of how satellite global field should be treated in regional precise geoid modelling. (Padding of terrestrial gravity data to improve Stokes-Helmert geoid computation). Geophysical Research Abstracts 17, EGU2015-6655-1, European Geoscience Union General Assembly, Vienna, Austria.

Foroughi I., Sheng M. B., Kingdon R. W., Huang J., Martinec Z., Vaníček P., Santos M. C., 2015b: The effect of lateral topographical density variations on the geoid in Auvergne. 26th IUGG General Assembly, Prague, Czech Republic.

Foroughi I., Vaníček P., Novák P., Kingdon R. W., Sheng M. B., Santos M. C., 2017a: Optimal Combination of Satellite and Terrestrial Gravity Data for Regional Geoid Determination Using Stokes-Helmerts Method, the Auvergne Test Case. In: International Association of Geodesy Symposia. Springer, Berlin, Heidelberg, `doi: 10.1007/1345_2017_22`.

Foroughi I., Vaníček P., Sheng M. B., Kingdon R. W., Santos M. C. 2017b: In defence of the classical heihgt system. Geophysical Journal International, **211**, 11761183, `doi: 10.1093/gji/ggx366`.

Helmert F. R., 1884: Die mathematischen und physikalischen Theorien der höheren Geodäsie, Band II, B. G. Treubner, Leipzig (in German).

Hensley S., Rosen P., Gurrola E., 2000: The SRTM topographic mapping processor. In: Geoscience and Remote Sensing Symposium IGRASS 2000. IEEE 2000 Int., **3**, 1168–1170.

Hörmander L., 1976: The boundary problems of physical geodesy. Arch. Ration. Mech. Anal., **62**, 1–52. `doi: 10.1007/BF00251855`.

Huang J., 2002: Computational Methods for the Discrete Downward Continuation of the Earth Gravity and Effedts of Lateral Topographical Mass Density Variation on gravity and The Geoid. University of New Brunswick, Fredericton, Canada.

Huang J., Sideris M. G., Vaníček P., Tziavos I. N., 2003: Numerical investigation of downward continuation techniques for gravity anomalies. Bollettino di Geodesia e Scienze Affini, **LXII**, 33–48.

Huang J., Vaníček P., Novák P., 2000: An alternative algorithm to FFT for the numerical evaluation of Stokes's integral. Stud. Geophys. Geod., **44**, 374–380.

Huang J., Vaníček P., Pagiatakis S., Brink W., 2001: Effect of topographical mass density variation on gravity and the geoid in the Canadian Rocky mountains. J. Geodesy, **74**, 805–815.

Janák J., Vaníček P., 2005: Mean free-air gravity anomalies in the mountains. Stud. Geophys. Geod., **49**, 31–42.

Kingdon R., Vaníček P., 2010: Poisson downward continuation solution by the Jacobi method. Journal of Geodetic Science, **1**, 74–81, `doi: 10.2478/v10156-010-0009-0`.

Lemoine F. G., Kenyon S. C., Factor J. K., Trimmer R. G., Pavlis N. K., Chinn D. S., Cox C. M., Klosko S. M., Luthcke S. B., Torrence M. H., Wang Y. M., Williamson R. G., Pavlis E. C., Rapp R. H., Olson T. R., 1998: The Development of the Joint NASA GSFC and the National Imagery and Mapping Agency (NIMA) Geopotential Model EGM96. NASA/TP-1998-206861.

MacMillan W., 1930: The Theory of Potential. Dover Publications, New York.

Martinec Z., 1993: Effect of lateral density variations of topographical masses in view of improving geoid model accuracy over Canada. Final report of contract DSS No. 23244-2-4356, Geodetic Survey of Canada, Ottawa.

Martinec Z., Vaníček P., 1994a: Direct topographical effect of Helmert's condensation for a spherical approximation of the geoid. Manuscr. Geodaet, **19**, 257–268.

Martinec Z., Vaníček P., 1994b: The indirect effect of topography in the Stokes-Helmert technique for a spherical approximation of the geoid. Manuscr. Geodaet, **19**, 213–219.

Martinec Z., Vaníček P., Mainville A., Véronneau M., 1995: The effect of lake water on geoidal heights. Manuscr. Geodaet, **20**, 193–203.

Martinec Z., Vaníček P., 1996: Formulation of the boundary-value problem for geoid determination with a higher degree reference field. Geophys. J. Int, **126**, 219–228.

Martinec Z., Vaníček P., Mainville A., Véronneau M., 1996: Evaluation of topographical effects in precise geoid computation from densely sampled heights. J. Geodesy, **70**, 746–754.

Martinec Z., 1998: Boundary-value problems for gravimetric determination of a precise geoid. Lecture Notes in Earth Sciences 73, Springer, Berlin.

Molodenskij M. S., Eremeev V. F., Yurkina M. I., 1960: Methods for study of the external gravitational field and figure of the Earth. Transl. from Russian by the Israel Program for Scientiffic Translations. Office of technical Services, Department of Commerce, Washington, D. C., 1962.

Novák P., 2000: Evaluation of gravity data for the Stokes-Helmert solution to the geodetic boundary-value problem. Technical Report No. 207, University of New Brunswick, Fredericton.

Novák P., Vaníček P., Véronneau M., Featherstone W. E., Holmes S. A., 2001: On the accuracy of modified Stokes's integration in high-frequency gravimetric geoid determination. J. Geodesy, **74**, 644–654.

Reuter H. I., Nelson A., Jarvis A., 2007: An evaluation of void filling interpolation methods for SRTM data. Int. J. Geogr. Inf. Sci., **21**, 983–1008.

227

Rodriguez E., Morris C. S., Belz J. E., Chapin E. C., Martin J. M., Daffer W., Hansley S., 2005: An assessment of the SRTM topographic products. Technical Report JPL D-31639, Jet Propulsion Laboratory, Pasadena, California.

Rülke A., Liebsch G., Sacher M., Schäfer U., Schirmer U., Ihde J., 2012: Unification of European height system realizations. Journal of Geodetic Science, **2**, 343–354.

Santos M. C., Vaníček P., Featherstone W. E., Kingdon R., Ellmann A., Martin B. A., Kuhn M., Tenzer R., 2006: The relation between rigorous and Helemert's definitions of orthometric heights. J. Geodesy, **80**, 691–704. `doi: 10.1007/s00190-006-0086-0`.

Sjöberg L. E., 2003: A computational scheme to model the geoid by the modified Stokes' formula without gravity reductions. J. Geod., **77**, 423–432.

Stokes G. G., 1849: On the variation of gravity at the surface of the earth. Trans. Cambridge Philos. Soc., **VIII**, 672–695.

Sun W., Vaníček P., 1998: On some problems of the downward continuation of $5' \times 5'$ mean Helmert's gravity disturbance. J. Geodesy, **72**, 411–420.

Tenzer R., Novák P., Janák J., Huang J., Najafi M., Vajda P., Santos M., 2003: A review of the UNB approach for precise geoid determination based on the Stokes-Helmert method. Honoring the academic life of Petr Vaníček. Technical Report **218**, University of New Brunswick, Fredericton, 132–176.

Vaníček P., Sjöberg L. E., 1991: Reformulation of Stokes's theory for higher than second-degree reference field and modification of integration kernels. J. Geophys. Res., **96**, B4, 6529–6539.

Vaníček P., Martinec Z., 1994: The Stokes-Helmert scheme for the evaluation of a precise geoid. Manuscr. Geodaet, **19**, 119–128.

Vaníček P., Najafi M., Martinec Z., Harrie L., Sjöberg L. E., 1995: Higher-degree reference field in the generalized Stokes-Helmert scheme for geoid computation. J. Geodesy, **70**, 176–182.

Vaníček P., Sun W., Ong P., Martinec Z., Najafi M., Vajda P., Horst B., 1996: Downward continuation of Helmert's gravity. J. Geodesy, **71**, 21–34.

Vaníček P., Featherstone W. E., 1998: Performance of three types of Stokes's kernel in the combined solution for the geoid. J. Geodesy, **72**, 684–697.

Vaníček P., Huang J., Novák P., Pagiatakis S., Véronneau M., Martinec Z., Featherstone W. E., 1999: Determination of the boundary values for the Stokes-Helmert problem. J. Geodesy, **73**, 180–192.

Vaníček P., Tenzer R., Sjöberg L. E., Martinec Z., Featherstone W. E., 2004: New views of spherical Bouguer gravity anomaly. Geophys. J. Int., **159**, 460–472. `doi: 10.1007/s00190-006-0086-0`.

Vaníček P., Kingdon R., Kuhn M., Ellmann A., Featherstone W. E., Santos M. C., Martinec Z., Hirt Ch., Avalos-Naranjo D., 2013: Testing Stokes-Helmert geoid model computation on a synthetic gravity field: experiences and shortcomings. Stud. Geophys. Geod., **57**, 369–400.

Werner M., 2001: Shuttle Radar Topography Mission (SRTM), Mission overview. J. Telecom (Frequenz), **55**, 75–79.

Yildiz H., Forsberg R., Ågren J., Tscherning C. C., Sjöberg L. E., 2012: Comparison of remove-compute-restore and least squares modification of Stokes' formula techniques to quasi-geoid determination over the Auvergne test area. Journal of Geodetic Science, **2**, 53–64, doi: 10.2478/v10156-011-0024-9.